UM-P-79/10

BREMSSTRAHLUNG AND NEUTRAL CURRENTS

R. G. Ellis* and Bruce H.J. McKellar

School of Physics, University of Melbourne,
Parkville, Victoria, Australia 3052

Abstract

The utility of the bremsstrahlung process in detecting parity violations from V-A weak neutral current interference is analysed in two ways. Firstly, bremsstrahlung from polarized lepton-nucleus scattering has an asymmetry with respect to the polarization of the incident leptons, and secondly, bremsstrahlung from unpolarized lepton nucleus scattering has a small circular polarization. The magnitude of each effect is calculated. The ratio of the parity violating contribution and the parity conserving contribution to the cross section is shown to be a misleading measure of the utility of these experiments. A parameter, the figure of merit, is introduced and used to discuss the feasibility of possible experiments.

---

*Work supported by a Commonwealth Postgraduate Research Award.

1. Introduction

Since the discovery of the neutral currents (CERN-GARGAMELLE collaboration, 1973) there have been many methods suggested for the determination of their structure (Adler et al., 1975, Pakvasa and Rajasekaran, 1975) yet several questions still remain unresolved. One of the most important questions is the nature of the neutral current interactions of the charged leptons. In particular, recent measurements of the parity-non-conserving (PNC) effect in atomic Bi (P. Baird, et al., 1976) which have been somewhat inconclusive, indicate that the PNC effect may be smaller than predicted by the Weinberg-Salam model (Loving, 1975). This model has been rather successful in the explanation of neutrino neutral current interactions (B.W. Lee, 1976) and in recent $e + d \rightarrow e' + X$ experiments (Prescott et al., 1978). Consequently further leptonic experiments to determine the magnitude of PNC neutral current effects would help resolve the nature of the weak currents.

To date a number of lepton-hadron and lepton-lepton systems have been investigated and experimental tests of PNC in neutral current couplings have been proposed involving $e(\text{polarized}) + d \rightarrow e' + X$ scattering (Prescott et al., 1978), electronic atoms (Bouchait and Bouchait, 1974, Brodsky and Karl, 1976) muonic atoms (Moskalev, 1974, Bernabeu et al., 1974, Feinberg and Chen, 1974), e^+e^- annihilation (Dass and Ross, 1975), lepton-lepton pair production (Mikaelian and Oakes, 1977) as well as circular polarization in bremsstrahlung (Jarlskog and Salomonson, 1976). We suggest an alternative method using lepton-nucleus bremsstrahlung as another process which may yield information about PNC due to neutral currents (McKellar, 1976).

In particular, the photon cross section for bremsstrahlung of polarized leptons on a nucleus will be asymmetric with respect to the polarization of the incident leptons if parity is not conserved.

The order of magnitude of this effect will be Gm_ℓ^2/α (McKellar, 1976), where m_ℓ is the mass of the polarized incident lepton: clearly PNC effects will be largest for muon bremsstrahlung.

The subsequent sections of this paper contain a calculation of the cross section for this process along with the magnitude of the PNC effect, and the designation of a new parameter, "the figure of merit", introduced in order to specify more accurately the viability of this and similar experiments. The figure of merit is then maximized to determine the optimum kinematic arrangement for the observation of PNC. Also included is a reanalysis of a proposed method for detection of PNC effects based on the PNC origin of circularly polarized photons resulting from unpolarized-lepton nucleus bremsstrahlung. This reanalysis is in terms of the figure of merit, and leads to somewhat different conclusions as to the optimum experimental conditions.

2. Calculation of the cross section.

We consider bremsstrahlung from a polarized muon in a point nucleus neglecting recoil corrections, to lowest order in perturbation theory. In the absence of neutral currents the appropriate Feynman diagrams are shown in figure 1 which give the parity conserving amplitude, (Sakurai, 1967).

$$M_{pc} = \frac{Ze^3}{Q^2}\,\bar{u}^{(s')}(p')\left[\gamma_4\,\frac{q\!\!\!/+im}{q^2+m^2}\,k\!\!\!/^{(\alpha)} + k\!\!\!/^{(\alpha)}\,\frac{q'\!\!\!/+im}{q'^2+m^2}\,\gamma_4\right]u^{(s)}(p) \qquad (2.1)$$

Where $\underset{\sim}{Q}$ is the 3-momentum transfer to the nucleus of charge Z, and the intermediate 4-momenta are $q = p - k$, $q' = p' + k$. p', p are the 4-momenta of the initial and final muons of mass m, and u and u' are the corresponding spinors. The metric, spinor normalization and notation are set out in Sakurai (1967).

Replacing the photon in figure 1 by the neutral weak boson Z^o yields the Feynman diagram for the neutral current contribution, figure 2. The interaction Lagrangian for the Z_o can be written,

$$L_{Z_o} = i \sum_{j=\mu,p,n} \bar{\psi}_j \gamma_\rho (a_j - b_j \gamma_5) \psi_j Z_{o_\rho} \tag{2.2}$$

where the summation is over the couplings of the Z_o to the muon and nucleons in the nucleus, with a_j and b_j being coupling constants. This yields the effective Lagrangian, L_{eff}, for the Z_o interaction shown in figure 3, as,

$$L_{eff} = i\bar{\psi}_\mu \gamma_\lambda (a_\mu - b_\mu \gamma_5) \psi_\mu \sum_{j'=p,n} \bar{\psi}_{j'} \gamma_\lambda (a_{j'} - b_{j'} \gamma_5) \psi_{j'} / m^2_{Z_o} \tag{2.3}$$

where we have taken the limit $Q^2 << m^2_{Z_o}$ where m_{Z_o} is the mass of the neutral boson, and the summation extends over all protons and neutrons in the nucleus.

If we assume an approximately random spin distribution amongst the nucleons, then the only term which will sum coherently will be,

$$\sum_{j'=p,n} \bar{\psi}_{j'} \gamma_4 \psi_{j'} a_{j'} = Z a_p + N a_n$$

where Z and N are the proton and neutron numbers of the nucleus, respectively.

Furthermore, taking only the parity violating part of L_{eff} we may write,

$$L_{eff_{pv}} = \frac{-ib_\mu}{m^2_{Z_o}} (Z a_p + N a_n) \bar{\psi}_\mu \gamma_4 \gamma_5 \psi_\mu . \tag{2.4}$$

Thus, the amplitude corresponding to the PNC part of figure 2 will be,

$$M_{pv} = -Ze^3\, \bar{u}'^{(s')}(p')\,\xi\, [\gamma_4\gamma_5 \frac{\not{q}+im}{q^2+m^2} \not{\epsilon}^{(\alpha)} + \not{\epsilon}^{(\alpha)} \frac{\not{q}'+im}{q'^2+m^2} \gamma_4\gamma_5]\, u^{(s)}(p) \tag{2.5}$$

where $\xi = \frac{1}{Ze^2} \frac{b_\mu}{m_{Z_o}^2} (Za_p + Na_n)$.

In the Weinberg-Salam model

$$\xi_{ws} = \frac{\sqrt{2}G}{4\pi\alpha} \{\mathrm{Sin}^2\sigma_w + \frac{N-Z}{4Z}\} \tag{2.6}$$

where θ_w, is the Weinberg angle, G and α are the Fermi and fine structure constants.

The magnitude of ξ_{ws} is typical of predictions made by other similar models, (Bjorken, 1977). Experimental attempts to determine ξ have been inconclusive, (Kayser, 1977), however, recent results from e(polarized) +d →e'+x inelastic scattering favour the W-S prediction, (Prescott et al, 1978).

The cross section resulting from the combination of the PC and PNC amplitudes is of the form

$$d\sigma = d\sigma_c \pm d\sigma_v \qquad \pm \text{ for } \mp \text{ ve helicity muons.}$$

Here, $d\sigma_c$ is the usual parity conserving cross section given by, (Koch and Motz, 1959).

$$d\sigma_c = \frac{2^2\alpha^3}{4\pi} \frac{|\underset{\sim}{p}'|}{|\underset{\sim}{p}|} \frac{d\omega\, d\Omega_k\, d\Omega_p, 2\omega^2}{\omega\, Q^4\, (cc')^2} \{-2cc'Q^2[2(E^2+E'^2)+c'+c-Q^2-2m^2]+$$

$$(c^2+c'^2)(cc'+2m^2Q^2)-8m^2(c'E'+cE)^2\} \tag{2.7}$$

Whilst, $d\sigma_v$ is the PNC contribution to the bremsstrahlung differential cross section, and is given by,

$$d\sigma_v = \frac{Z^2\alpha^3 2\xi |\tilde{p}'| d\omega\ d\Omega_k d\Omega_{p'} \omega^2}{\pi \quad |\tilde{p}|\ \omega\ Q^2} \left\{ \frac{1}{c'}(EQ^2+E'm^2+2Em^2 - \frac{Ec}{2}) + \right.$$

$$\frac{1}{c}(EQ^2+Em^2+3E'm^2 - \frac{c'E}{2}) + \frac{1}{cc'}[(Q^2+2m^2)(-EQ^2+2p^2(E+E')-2EE'\omega)-m^2Q^2\omega]$$

$$\left. + \frac{E}{c'^2}\ m^2(4p^2-Q^2) + \frac{1}{c^2}[m^2E'(4p'^2-Q^2)+4m^2EE'\omega+Ec'm^2] \right\} \qquad (2.8)$$

and $\quad c = -2p.k = 2(E\omega - p\omega\cos\theta)\ ;\ c' = 2p'.k = -2(E'\omega - p'\omega\cos\theta')$

and $\quad Q^2 = |\tilde{p}-\tilde{p}'-\tilde{k}|^2 = p^2+p'^2+\omega^2-2p\omega\cos\theta+2p'\omega\cos\theta'-2pp'(\cos\theta\cos\theta'+$

$$\cos\phi\sin\theta'\sin\theta).$$

The angles θ, θ', ϕ are defined in figure 4. Integrating over the angie coordinates θ' and ϕ of the scattered muon yields the differential cross section in photon energy and direction $d\sigma(\hat{k},\omega)$ which can again be separated in PC and PNC components.

$$d\sigma(\hat{k},\omega) \equiv d\sigma_c(\hat{k},\omega) \pm d\sigma_v(\hat{k},\omega)$$

where $\quad d\sigma_c(\hat{k},\omega) = \frac{Z^2\alpha^3}{\pi}\ \frac{d\omega}{\omega}\frac{d\Omega_k}{m^2}\frac{p'}{p}\ \omega^2\left\{\frac{m^4 16\omega^2\sin^2\theta\ (2E^2+m^2)}{p^2c^4} - m^2\frac{(p^2-\omega^2)}{T^2c^2} + \right.$

$$\frac{E'm^2}{p^2c\omega} - \frac{m^2(5E^2+2EE'+3m^2)}{p^2c^2} + \frac{L}{pp'}\left[\frac{8m^4E\omega^2\sin^2\theta(3\omega m^2-p^2E')}{p^2c^4} + \frac{2m^2E^2(E^2+E'^2)}{p^2c^2}\right.$$

$$\left. + \frac{m^2(E^2+EE'-m^2)}{2p^2c^2}\right] - \frac{m^2\varepsilon}{p'c\omega} + \frac{Lm^4}{p^3p'c^2}[m^2-7E^2+3EE'-E'^2] + \varepsilon^T\left[\frac{4m^2}{c^2} - \frac{3}{c} - \right.$$

$$\left. \left. - \frac{(p^2-\omega^2)}{T^2c}\right]\right\} \qquad (2.9)$$

and the parity violating contribution yields -

$$d\sigma_v(\hat{k},\omega) = \frac{Z^2\alpha^3}{\pi}\,\xi\,\frac{d\omega}{\omega}\;d\Omega_k\;2\omega^2\,\frac{p'}{p^2}\,\{\frac{\varepsilon E}{c\omega p'}\,[\frac{E'c}{\omega} + m^2(5+\frac{E'}{E}) - 2(E^2+E'^2+m^2)]+$$

$$\frac{\varepsilon^T m^2}{cp'T}\,[2E+6E'+\frac{8}{c}\,(E'p'^2+EE'\omega)+\frac{E}{2T^2m^2}(c-2m^2)(c-2m^2+2EE')] + \frac{4Lm^2}{p'pc^2}[2EE'\omega+Ep'^2-$$

$$p^2E - E'p^2 - \frac{Ec}{2} + \frac{Ec^2}{8m^2}\,] - \frac{3E}{\omega^2} + \frac{4E^2}{\omega c} - \frac{4E'm^2}{c^2} - \frac{8Em^2}{c^2} + \frac{2E}{T^2c}(c-2E'\omega)(\frac{m}{c}-\frac{1}{2}) -$$

$$\frac{4E}{\omega cp'^2}\,[\omega m^2 - E'(EE'-m^2)]$$

where $\varepsilon = \ln(\frac{E'+p'}{E'-p'})$; $\varepsilon^T = \ln(\frac{T-p'}{T-p'})$; $T = |\underset{\sim}{p} - \underset{\sim}{k}| = \sqrt{p'^2+c}$;

$$L = \ln(\frac{EE'-m^2+pp'}{EE'-m^2-pp'}). \qquad (2.10)$$

The results of these calculations are shown in figure 5 where $d\sigma_c(\hat{k},\omega)$ and $d\sigma_v(\hat{k},\omega)$ are drawn on the same axes to illustrate the magnitude of the PNC effect, for a muon of energy 3 Gev and photon energy 1.5 and 0.5Gev.

In figure 6 we show the ratio, R_γ, of the PNC and PC contribution to the differential photon cross section, ie.-

$$R_\gamma(\hat{k},\omega) = \frac{\int\int_{\Delta\omega\Delta\Omega_k} d^2\sigma_v(\hat{k},\omega)}{\int\int_{\Delta\omega\Delta\Omega_k} d^2\sigma_c(\hat{k},\omega)} \qquad (2.11)$$

Where the intergrals are over the element $(\Delta\Omega_k,\Delta\omega)$ about $(\hat{k},\omega)$. $R_\gamma(\hat{k},\omega)$ is the parameter usually associated with the feasibility of process yielding experimental information about PNC effects. We have

included it for comparison with other calculations but emphasize that R_γ is not a true indication of the experimental feasibility of the process under consideration. Instead we introduce another parameter, "the figure of merit", which is a more realistic measure of the observability of PNC effects.

3. THE FIGURE OF MERIT.

Measurements of the PNC effects require the determination of the different ΔN between the number of photons observed with one orientation of muon spin and the number with the other orientation. If N is the total number of photons observed in solid angle $\Delta\Omega_k$ and in energy range $\Delta\omega$ about ω then-

$$\Delta N \simeq \frac{N\epsilon \int\int_{\Delta\Omega_k \Delta\omega} d^2\sigma_v}{\int\int_{\Delta\Omega_k \Delta\omega} d^2\sigma_c} \qquad (3.1)$$

Where ϵ is the degree of muon polarization. To establish the existence of a real effect as distinct from a statistical fluctuation we require-

$$\Delta N \gtrsim N^{\frac{1}{2}}$$

or

$$\epsilon \frac{\int\int_{\Delta\Omega_k \Delta\omega} d^2\sigma_v}{\int\int_{\Delta\Omega_k \Delta\omega} d^2\sigma_c} N^{\frac{1}{2}} \gtrsim 1 \qquad (3.2)$$

Further, the total number of photons, N, can be related to the number of incident muons N_μ by-

$$N = N_\mu \int_{\Delta\Omega_k} \int_{\Delta\omega} d^2\sigma_c \; N_A . t. \tag{3.3}$$

Where N_A is the number of atoms per urit volume of the target material and t is the thickness of the target.

Substituting (3.3) into (3.2),

$$F_\gamma \equiv \frac{\iint_{\Delta\omega\Delta\Omega_k} d^2\sigma_v}{\left| \iint_{\Delta\omega\Delta\Omega_k} d^2\sigma_c \right|^{\frac{1}{2}}} \geq \frac{1}{\varepsilon \sqrt{N_\mu N_A . t . \varepsilon'}} \tag{3.4}$$

Where $\Delta\Omega_k$, Δw becomes the solid angle of acceptance and energy resolution of the photon detector, and ε' has been introduced as the detector efficiency.

We define the LHS as the "figure of merit", F_γ, for this experimental situation and observe that maximization of F_γ corresponds to the optimum kinematic arrangement for the observation of PNC effects. The kinematic arrangement obtained in this way is quite different to that suggested by maximizing R_γ which is the more usual procedure.

In order to evaluate the figure of merit it is necessary to intergrate $d^2\sigma_v$ over $\Delta\Omega_k$. Explicitly,

$$\int \frac{d\sigma_v}{d\Omega_k d\omega} d\Omega_k = \int \frac{d\sigma_v}{d\Omega_k d\omega} 2\pi \mathrm{Sin}\theta d\theta = Z^2\alpha^3 \frac{2\omega}{p^2} \left\{ \frac{2EE'\epsilon}{\omega^2} \cos\theta + \right.$$

$$\frac{\ell nc.\epsilon E}{p\omega^2}(2(E^2+E'^2+m^2)-m^2(5+\frac{E'}{E})) + \frac{\epsilon T^2 m^2}{p'p\omega}(E+3E') + \frac{8m^2}{pp'\omega}(-\frac{\epsilon^T}{4p'^2} +$$

$$+ \frac{T\epsilon^T}{p'(T^2-p^2)} -$$

$$\frac{(E'p'^2+EE'\omega)}{(T^2-p'^2)} + \frac{4m^2E}{pp'^2\omega}(\frac{\epsilon^T}{T} - \frac{\epsilon^T}{4p'} + \frac{\delta}{p'})(EE'-m^2) - \frac{E}{p\omega}((T-p' + \frac{p'^2}{T})\epsilon^T +$$

$$2p'\ell n(\frac{T+p'}{p}) + p'\delta) + \frac{E}{p\omega}(\frac{\epsilon^T}{T} + \frac{\delta}{p'})(2EE'-4m^2) + \frac{4Lm^2}{p^2\omega c}(2EE'\omega+Ep'^2-p^2E-E'p^2)$$

$$+ \frac{2ELm^2}{p^2\omega}\ell nc + 2\cos\theta(\frac{LE}{2p} - \frac{3p'E}{\omega^2}) - \frac{4p'E^2}{\omega^2 p}\ell nc - \frac{4p'm^2}{p\omega c}(E'+2E) - \frac{2E\delta}{pp'\omega}(E'\omega+m^2)$$

$$+ \frac{2p'E}{p\omega}\ell nT + \frac{4\pi EE'}{pp'^3}(\frac{p'^2}{(T^2-p'^2)} + \delta) + \frac{4E\ell nc}{p\omega^2 p'}(\omega m^2 - E'(EE'-m^2)) \Big\} \qquad (3.5)$$

and

$$\int \frac{d\sigma_c}{d\Omega_k d\omega} 2\pi \mathrm{Sin}\theta d\theta = Z^2\alpha^3 \frac{p'}{p} \left\{ \frac{8m^2\omega^2}{c^3}(2m^2+4E^2+\frac{LE}{pp'}(3m^2\omega-p^2E')(\frac{1}{3} - \right.$$

$$\mathrm{Cos}^2\theta + \frac{E\cos\theta}{p} - \frac{E^2}{3p^2}) - \frac{5E^2+2EE'+3m^2}{c} + \frac{2E^2L}{pp'c}(E^2+E'^2) +$$

$$+ \frac{m^4L}{pp'c}(m^2-7E+3EE'-E'^2)$$

$$+ (\frac{\epsilon p^2}{p'\omega} - \frac{E'}{\omega} + \frac{(E^2+EE'-m^2)L}{2pp'}) + \frac{(p^2-\omega^2)}{p'^4}p^2(\frac{p'^2}{(T^2-p'^2)}+\delta) + \frac{2m^2T\epsilon^T p^2}{p'^3(T^2-p'^2)} -$$

$$- \frac{m^2\epsilon^{T^2}p^2}{2p'^4}$$

$$- \frac{2m^2p^2}{p'^2(T^2-p'^2)} - \frac{3\epsilon^{T^2}p^2}{4p'^2} + \frac{(p^2-\omega^2)}{p'^3}p^2(\frac{\delta}{p'} - \frac{\epsilon^T}{T} - \frac{\epsilon^{T^2}}{4p'^2}) \qquad (3.6)$$

where $\delta = \ell n \left(\frac{T^2-p'^2}{T^2}\right)$

As a typical case the figure of merit has been plotted in figure 7 for muons of energy 3Gev, photon energy 1.5 and 0.5Gev with energy range $\Delta\omega$ = 0.05Gev and small solid angle $\Delta\Omega_k = \pi/_{20}$sr.

Comparison of figure 6 and figure 7 show that for the same conditions the maxima of F_γ and R_γ occur at significantly different values of θ. Maximization of R_γ is misleading and use of the figure of merit is necessary for proper optimization of the kinematic arrangement of the experimental situation.

Maximization of $F_\gamma\ (\hat{k},\omega,\Delta\Omega_k\ \Delta\omega)\big|_{\epsilon = 3Gev}$ indicates that the optimum kinematic arrangement occurs for observation of the complete photon energy range and photons in solid angle $\Delta\Omega_k$ extending from polar angle $\theta = 40^o$ to 180^o and all azimuthal angles ϕ. The figure of merit is shown for several different solid angles in figure 8 which yields,

$$F_{\gamma_{max}}\big|_{3Gev} = Z\,\xi \times 2.16\times10^{-2} \qquad (3.7)$$

Rearranging (3.4),

$$N_{\mu_{min}} \geq \frac{1}{\epsilon^2 F_{\gamma_{max}}^{\ 2}\ N_a t\ \epsilon'} \qquad (3.8)$$

$N_{\mu_{min}}$ is approximately inversely proportional to Z since F_γ is proportional to Z and N_a is approximately inversel, proportional to Z. Thus, a high Z target material will increase the feasibility of this experiment.

The following typical values can be used to estimate $N_{\mu_{min}}$,

(i) ϵ, the degree of polarization of the incident muons $\sim$ 90%

(ii) ϵ, the photon detector efficiency $\sim$ 20%

(iii) N_a, for a Pb target $\sim 3.3 \times 10^{22}$ cm^{-3}

(iv) t, target thickness $\sim 10^2$ cm

(v) ξ, from the Weinberg-Salam model ($\sin^2\theta_w = 0.25$) $\sim$ $\sim 6.91 \times 10^{-5}$ Gev^2

giving

$$N_{\mu_{min}} \geq 3.2 \times 10^{11} \qquad (3.9)$$

Thus, maximization of the figure of merit has given the minimum number of muons required in order to observe a statistically significant PNC effect, as well as determining the optimum kinematic arrangement for this observation.

4. FORMFACTOR EFFECTS.

Formfactor effects are expected to be significant in muon bremsstrahlung. The formfactor can be included by replacing,

$$\int_\omega \int_\Omega d\sigma \qquad \text{with} \qquad \int_\omega \int_\Omega F(Q^2) d\sigma$$

Where $F(Q^2)$ is the formfactor. Analytical treatment becomes difficult with the inclusion of the formfactor and the results of a numerical analysis are shown in figures 6 and 7. The dipole type formfactor

$$F(Q^2) = \left(\frac{m^2}{m^2+Q^2}\right)^2 \qquad \text{where} \quad m^2 = 0.71 \ \text{Gev}^2$$

was used and is at least approximately verified at low Q^2 by existing data. (Schreiner, 1974), (Kirk et al, 1973, Hanson et al, 1973, Bartel et al, 1973). Maximization of the figure of merit $F_\gamma(\hat{k}, \omega, \Delta\Omega_k, \Delta\omega)|_{E=3\text{Gev}}$ with the formfactor included, indicates that the optimum kinematic arrangement for the detection of a photon asymmetry occurs for observation of the complete photon energy range and photons in solid

angle $\Delta\Omega_k$ extending from polar angle $\theta=8^\circ$ to 148° and all azimuthal angles, ϕ. The figure of merit with the formfactor included is shown in figure 8 for the optimum solid angle. This yields,

$$F_{\gamma_{max}}\Big|_{\substack{3Gev \\ (FF)}} = Z\,\xi \times 1.8 \times 10^{-3}$$

which gives,

$$N_{\mu_{min_{FF}}} \geq 4.6 \times 10^{13}$$

Hence detection of a statistically significant PNC effect requires at least 4.6×10^{13} muons. It remains to be seen if $N_\mu \sim 5\times10^{13}$ is experimentally feasible.

5. CIRCULAR POLARIZATION OF ELECTRON BREMSSTRAHLUNG.

A reanalysis has been made of a related calculation by Jarlskog and Salomonson in terms of the figure of merit. They have calculated the magnitude of circular polarization of bremsstrahlung from unpolarized lepton-nucleus scattering. This circular polarization has its origin in the PNC interaction. Figures 9 and 10 show the figure of merit, F_{JS}, and the circular polarization, R_{JS}, which is the difference between the right circularly polarized cross section, $d\sigma_R$ and the left circularly polarized cross section, $d\sigma_L$, over the total cross section. ie,

$$R_{JS} \equiv \frac{d\sigma_R - d\sigma_L}{d\sigma_R + d\sigma_L} \qquad (5.1)$$

Figures 9 and 10 are shown for 30 Mev electrons with bremsstrahlung photon energy 15 Mev ± 0.75 Mev and 6 Mev ± 0.75 Mev and solid angle of acceptance $\Delta\Omega_k = \frac{\pi}{20}$ sr. In this case figure 10 indicates that the optimum kinematic arrangement for the observation of circular polarization will be with the detector centre at about 12° from

the forward direction. At this position R_{JS} is about 2% of maximum, thereby illustrating the necessity of a figure of merit calculation to optimize the experimental arrangement.

The figure of merit has been maximized with respect to solid angle and photon energy range and the results shown in figure 11. The optimum kinematic arrangement occurs for observation of the complete photon energy range and photons in the solid angle, $\Delta\Omega_k$, extending from polar angle, θ, between 30^o and 180^o and all azimuthal angles ϕ (cf figure 4).

From figure 11,

$$F_{JS_{max}} = Z\,\xi \times 6.13 \times 10^{-5}\ \text{Gev}^{-1}$$

In this type of experiment equation (3.8) becomes

$$N_{\mu_{min}} \geq \frac{1}{\epsilon_{JS}^2 \epsilon'_{JS}\, F_{JS_{max}}\, N_a t}$$

where (i) ϵ_{JS} = polarization analysing efficiency $\sim$ 5%

(ii) ϵ'_{JS} = photon detector efficiency $\sim$ 20%

For a Pb target with thickness 1mm

$$N_{\mu_{min}} \geq 1.3 \times 10^{22}$$

Again, maximization of the figure of merit has given the optimum kinematic arrangement for observation of PNC effects. In this case the minimum number of electrons required to ensure that the PNC effect will be significant has been estimated to be 1.3×10^{22}. With a beam current of 300 μA, this would take approximately 2,000 hours.

Formfactor effects will not be significant at 30Mev because

of the much lower momentum transfer than in the previous calculation involving muons.

6. CONCLUSION.

The feasibility of two experiments which could yield significant information on the nature of the neutral current interaction of charged leptons has been analysed.

The first of these experiments involved detection of an asymmetry in the bremsstrahlung photon cross section with respect to the helicity of a polarized incident beam of muons. It was shown that at least 4.6×10^{13} 3Gev muons would be required for the asymmetry to be statistically significant.

The second of these experiments (previously considered by Jarlskog and Salomonson) involves the detection of circular polarization in the bremsstrahlung photon cross section from unpolarized electrons. It was shown that at least 1.3×10^{22} 30Mev electrons would be required for statistical significance. The existence of the asymmetry and circular polarization which these experiments respectively attempt to detect are PNC in origin.

It should be emphasized that these calculations made on the basis of maximization of the figure of merit, yield the minimum number of leptons required for detection of a statistically significant PNC effect. Clearly in most experimental situations greater lepton intensities will be required if the conditions for maximization of the figure of merit cannot be experimentally achieved. However, a smaller number of leptons than specified cannot yield any significant information.

In conclusion, the detection of PNC effects of neutral current V - A interference in bremsstrahlung would considerably stretch the

present state of the art. Whether either of these experiments are feasible remains to be seen. In this paper, one criterion, the required number of incident leptons, has been calculated and this must be satisfied before further investigation using either of these two experiments should be undertaken.

APPENDIX.

This appendix contains the equations used in the calculation of the figure of merit, F_{JS}, and the ratio R_{JS}, for the circular polarization experiment.

The matrix elements and Feynman diagrams will be the same as expression and figure 2. The cross section resulting from combination of the parity conserving and parity violating amplitudes will have the form,

$$d\sigma = d\sigma_R + d\sigma_L$$

where $d\sigma_R$ is the right hand polarized photon cross section and $d\sigma_L$ is the left hand polarized cross section. A difference in $d\sigma_R$ and $d\sigma_L$ indicates parity violation. Hence in this case,

$$d\sigma_{v_{JS}} = d\sigma_R - d\sigma_L \quad \text{while} \quad d\sigma_{c_{JS}} = d\sigma_R + d\sigma_L$$

where $d\sigma_v$ is parity violating in origin and $d\sigma_c$ is just the total bremsstrahlung cross section which will be the same as in the asymmetry calculation.

Squaring the amplitudes yields-

$$d\sigma_{v_{JS}} = -\frac{Z\alpha^3}{\pi^2}\frac{|p'|}{|p|}\xi\frac{d\omega}{\omega}\frac{d\Omega_k d\Omega p'}{Q^2}\omega^2\left\{2m^2(c-c')\left(\frac{1}{c'}+\frac{1}{c}\right)^2 -\right.$$

$$\left. 8m^2\omega\left(\frac{1}{c'}+\frac{1}{c}\right)\left(\frac{E}{c'}+\frac{E'}{c}\right)+\frac{2Q^2}{cc'}\left[c-c'-2(E^2-E'^2)\right]-\frac{1}{cc'}\left(c^2-c'^2\right)\right\}$$

in analogy with equation (2.8)

Intergrating over the angles of the scattered electron yields (c.f. equation 2.10)

$$d\sigma_{v_{JS}}(\hat{k},\omega) = -\frac{Z^2\alpha^3}{\pi}\,\xi\,\frac{d\omega}{\omega}\,d\Omega_k\,\frac{2p'}{p}\,\omega^2\{\frac{2m^2}{p'^2p^2}\{-\frac{(c+2p'^2)}{c}+\frac{(EE'-m^2)}{m^2\omega}E'+$$

$$\frac{c+2(EE'-m^2)}{2c}\,\frac{p'}{p}\,L] - \frac{8m^2\omega E}{p'^2p^2}\,[\frac{-c+2p'^2}{c^2}+\frac{(EE'-m^2)}{m^2\omega c}E' + \frac{c+2(EE'-m^2)}{2c^2}\,\frac{p'}{p}\,L\,] -$$

$$\frac{2m^2}{T^2}\,(\frac{2(c-E'\omega)}{c^2}-\frac{c+2(EE'-m^2)\varepsilon^T}{p'Tc}+\frac{2(c-E'\omega)}{cT^2}-\frac{(c+2(EE'-m^2))\varepsilon^T}{p'T^3})-\frac{L}{pp'}\,($$

$$\frac{2m^2}{c}-\frac{8m^2\omega(E+E')}{c^2}\,-1)+\frac{4}{p'}\,(-\frac{m^2\varepsilon^T}{cT}-\frac{4m^2\omega E'\varepsilon^T}{c^2T})-\frac{2\varepsilon}{\omega p'}\,(1-\frac{2}{c}(E^2-E'^2))-\frac{8}{c}\}$$

Integrating $d\sigma_{v_{JS}}(\hat{k},\omega)$ over $\Delta\Omega_k$, (cf equation (3.5)). $\int \frac{d\sigma_{v_{JS}}}{d\Omega_k d\omega}\,2\pi \mathrm{Sin}\theta d\theta =$

$$= Z^2\alpha^3\,\xi\,\frac{d\omega}{\omega}\,d\Omega_k\,\frac{8p'}{p}\,\omega^2\,\{\frac{m^2}{p'p^3}\,(-\frac{p}{p'}\cos\theta+\frac{p'}{\omega}\,\ell nc+\frac{E'p}{p'}\,\frac{(EE'-m^2)}{m^2\omega}\cos\theta$$

$$+\frac{L}{2}\cos\theta-\frac{L}{2\omega p}\,(EE'-m^2)\,\ell nc)-\frac{2m^2E}{p'^2p^3}\,(\ell nc-\frac{2p'^2}{c}-\frac{(EE'-m^2)}{m^2\omega}\,E'\,\ell nc$$

$$-\frac{p'L}{2p}\,\ell nc+\frac{(EE'-m^2)}{cp}\,p'L)-\frac{\varepsilon^T2m^2}{2p'^2\omega p}-\frac{4m^2E'}{pp'^4}\,(-\frac{\varepsilon^T2}{4}+\frac{T\varepsilon^Tp'}{(T^2-p'^2)}-$$

$$-(\frac{p'^2}{T^2-p'^2}))$$

$$-\frac{L}{pp'}\,(-\frac{m^2}{2p\omega}\,\ell nc-\frac{2m^2(E+E')}{pc}\,-\frac{\cos\theta}{2})-\frac{\varepsilon}{\omega p'}\,(\frac{\cos\theta}{2}+\frac{(E^2-E'^2)\,\ell nc}{p\omega})+$$

$$+\frac{m^2\delta}{pp'^2\omega}$$

$$-\frac{m^2E'}{pp'^4}\,[\frac{p'^2}{(T^2-p'^2)}+\delta]+\frac{m^2}{p'p\omega}\,[\frac{\varepsilon^T}{T}+\frac{\delta}{p'}]-\frac{m^2}{p'^4p\omega}\,(EE'-m^2)[-\frac{\varepsilon^T2}{4}+$$

$$+\frac{p'}{T}\,\varepsilon^T+\delta]$$

$$- \frac{\ell nT}{p\omega} + \frac{E'\delta}{2pp'z} + \frac{1}{2p'p\omega}\left((T+p')\ \ell n\ (T+p')-(T+p')+ \frac{p'^2}{T}\ \epsilon^T + p'\delta\right)-$$

$$- \left(\frac{EE'-m^2}{p\omega p'}\right)\left(\frac{\epsilon^T}{T} + \frac{\delta}{p'}\right) - \frac{2}{p\omega}\ \ell nc\ \Big\}$$

These expressions together with the parity conserving equations (2.7), (2.9), (3.6) are sufficient to evaluate $R_{\gamma_{JS}}$ and $F_{\gamma_{JS}}$.

References

S.L. Adler et al 1975 Phys. Rev. D12 3522

P. Baird et al 1976 Nature (London) 264, 528

W. Bartel et al 1973 Nucl Phys. B58, 429

J. Bernabeu et al 1974 Phys. Lett. 50B, 467

J.D. Bjorken 1977 Preprint SLAC-PUB 1866

C.C. Bouchait and M.A. Bouchait 1974 Phys. Letts. 48B, 111

S.J. Brodsky and G. Karl 1976 Comm. At. and Mol. Phys. 5, 63

CERN-GARGAMELLE collab. 1973 Phys. Letts. 46B, 121

G.V. Dass and G.C. Ross 1975 Phys. Letts. 57B, 1973

G. Feinberg and M.Y. Chen 1974 Phys. Rev. D10, 190, 3789

K.M. Hanson et al 1973 Phys. Rev. D8, 753

E. Henley and L. Wilets 1976 Phys. Rev. A14, 1411

C. Jarlskog and P. Salomonson 1976 Nucl. Phys. B107, 285

B. Kayser 1977 Phys. Rev. D15, 3407

P.N. Kirk et al 1973 Phys. Rev. D8, 63

H.W. Koch and J.W. Motz 1959 R.M.P. 31, 920

B.W. Lee 1976 at the Aachen Neutrino Conference Preprint FERMILAB-conf.-76/61THY

C. Loving and P. Sanders 1975 J. Phys. B8, L336

B.H.J. McKellar 1976 Lett. Nuovo Cim. 17, 481

K.O. Mikaelian and R.J. Oakes 1977 Phys. Letts. 70B, 358

A.N. Moskalev 1974 JETP Letts. 19 229, 394

S. Pakvasa and G. Rajasekaran 1975 Phys. Rev. D12, 113

C.Y. Prescott et al 1978 Phys. Letts. 77B, 347

J.J. Sakurai 1967, "Advanced Quantum Mechanics", Addison-Wesley

P.A. Schreiner 1974 Neutrino - Proc. 4th International Conference on Neutrino Physics and Astrophysics Philadelphia, ed. C. Battay (A.I.P. New York)

Figure Captions

Fig. 1.

Lowest order diagrams contributing to electromagnetic bremsstrahlung. ⊛ represents the nucleus.

Fig. 2.

Lowest order diagrams contributing to parity non conserving matrix elements in bremsstrahlung. The cross represents the nucleus and the dot the neutral current interaction. Z_o is the neutral intermediate vector boson.

Fig. 3.

Feynman diagram for the interaction betwen the muon and the nucleon via the intermediate vector boson, Z_o. In the static limit this reduces to the neutral current interaction of Fig. 2.

Fig. 4.

Defines the angles θ, θ',ϕ. $\underset{\sim}{p}$, $\underset{\sim}{p}'$, $\underset{\sim}{k}$ are the incident muon momentum, the scattered muon momentum and the photon momentum respectively.

Fig. 5.

Illustrates the relative magnitude of $\int\int_{\Delta\Omega_k \Delta\omega} d\sigma_c = PC$

and $\int\int_{\Delta\Omega_k \Delta\omega} d\sigma_v = PV$ where the integral is

over $\Delta\omega = 0.05$ GeV $\omega = \underline{1},\underline{2}$ GeV $\Delta\Omega_k = \frac{\pi}{20}$ sr and E = 3GeV.

Fig. 6.

R_γ as a function of polar angle θ; $\Delta\omega = 0.05$ GeV

$\Delta\Omega_k = \frac{\pi}{20}$ sr. $\omega = 1.6$, 0.6 GeV E = 3GeV.

Figure Captions (Contd.)

Fig. 7.

F_γ as a function of θ. ; $\Delta\omega, \Delta\Omega_k, \omega, E$ as in Fig. 6.

Fig. 8.

Maximization of F_γ as a function of solid angle magnitude and direction. The curve labelled 140_{FF} corresponds to maximization of F_γ with formfactor included. The labels 3, 30, 60, 90 etc. correspond to the polar angle $\Delta\theta$, over which $\Delta\Omega_k$ extends. θ defines the angle about which $\Delta\Omega_k$ is centred.

Fig. 9.

$R_{\gamma_{JS}}$ as a function of θ. $E = 30MeV$ $\Delta\omega = 0.75$ MeV

$$\Delta\Omega_k = \frac{\pi}{20} \text{ sr} \quad \omega = 15, 6$$

Fig. 10.

$F_{\gamma_{JS}}$ as a function of θ. E, $\Delta\omega$, $\Delta\Omega_k$, ω as in Fig. 9.

Fig. 11.

$F_{\gamma_{JS}}$ maximized as a function of solid angle magnitude and direction. The labels 3, 30, 60 etc., as in Fig. 8.

Fig. 1.

Fig. 2.

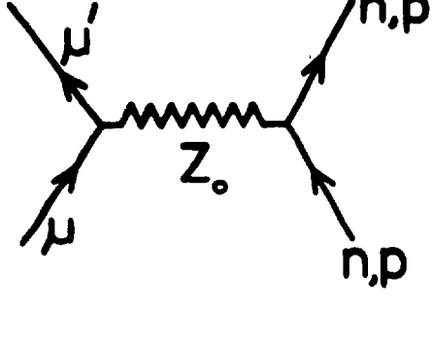

Fig . 3 .

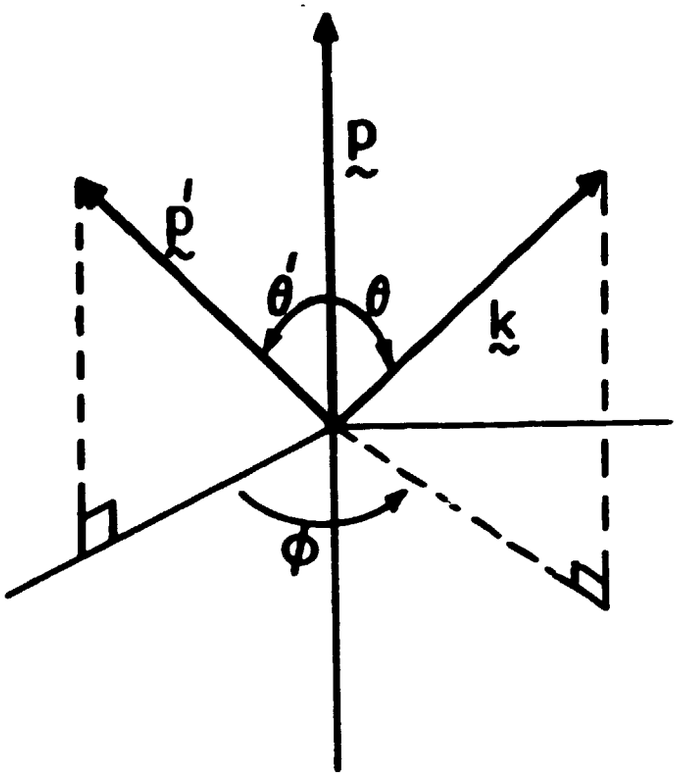

Fig. 4.

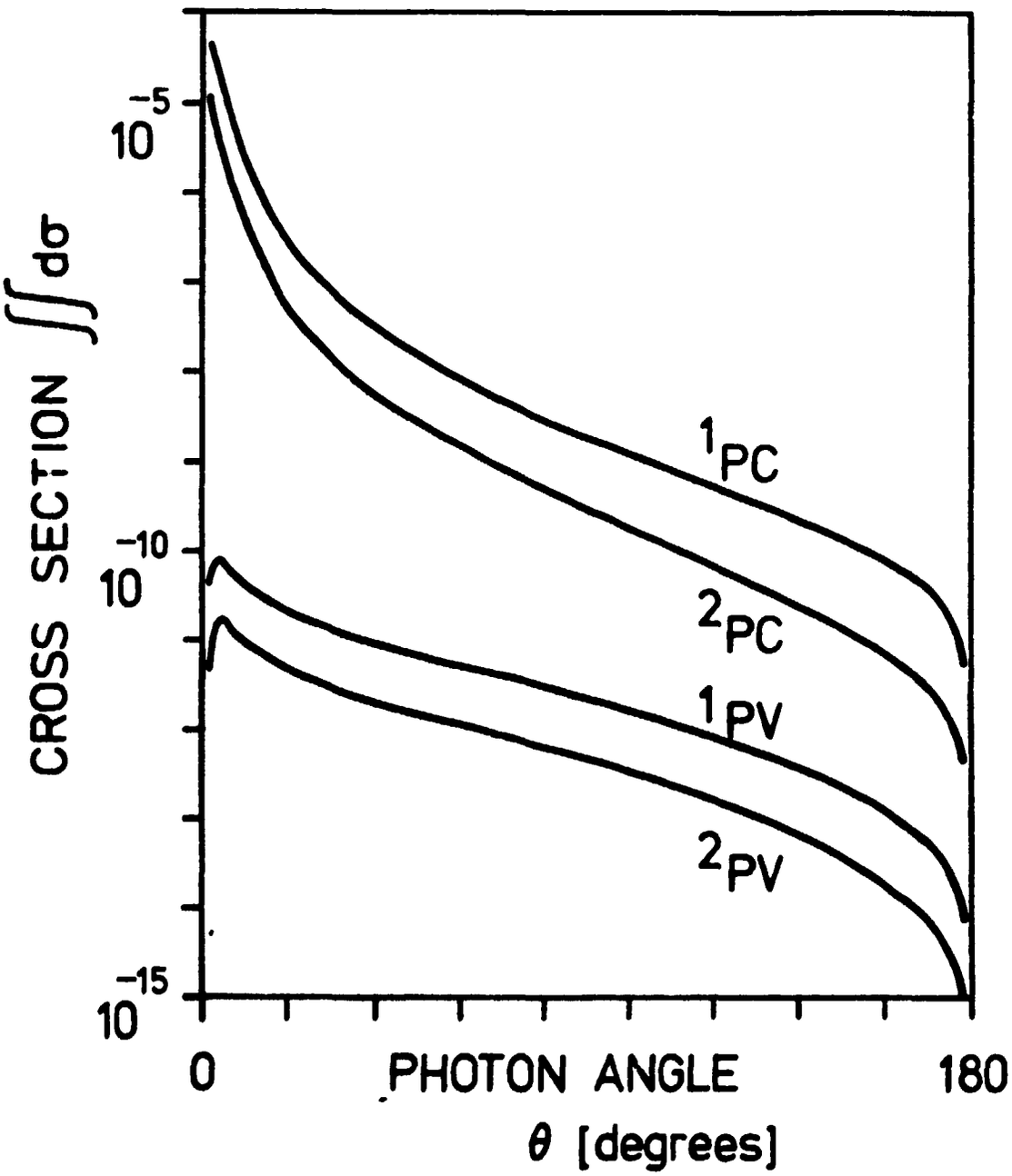
CROSS SECTION ∫∫dσ
10^-5
10^-10
10^-15
1PC
2PC
1PV
2PV
0
PHOTON ANGLE
180
θ [degrees]

Fig. 5.

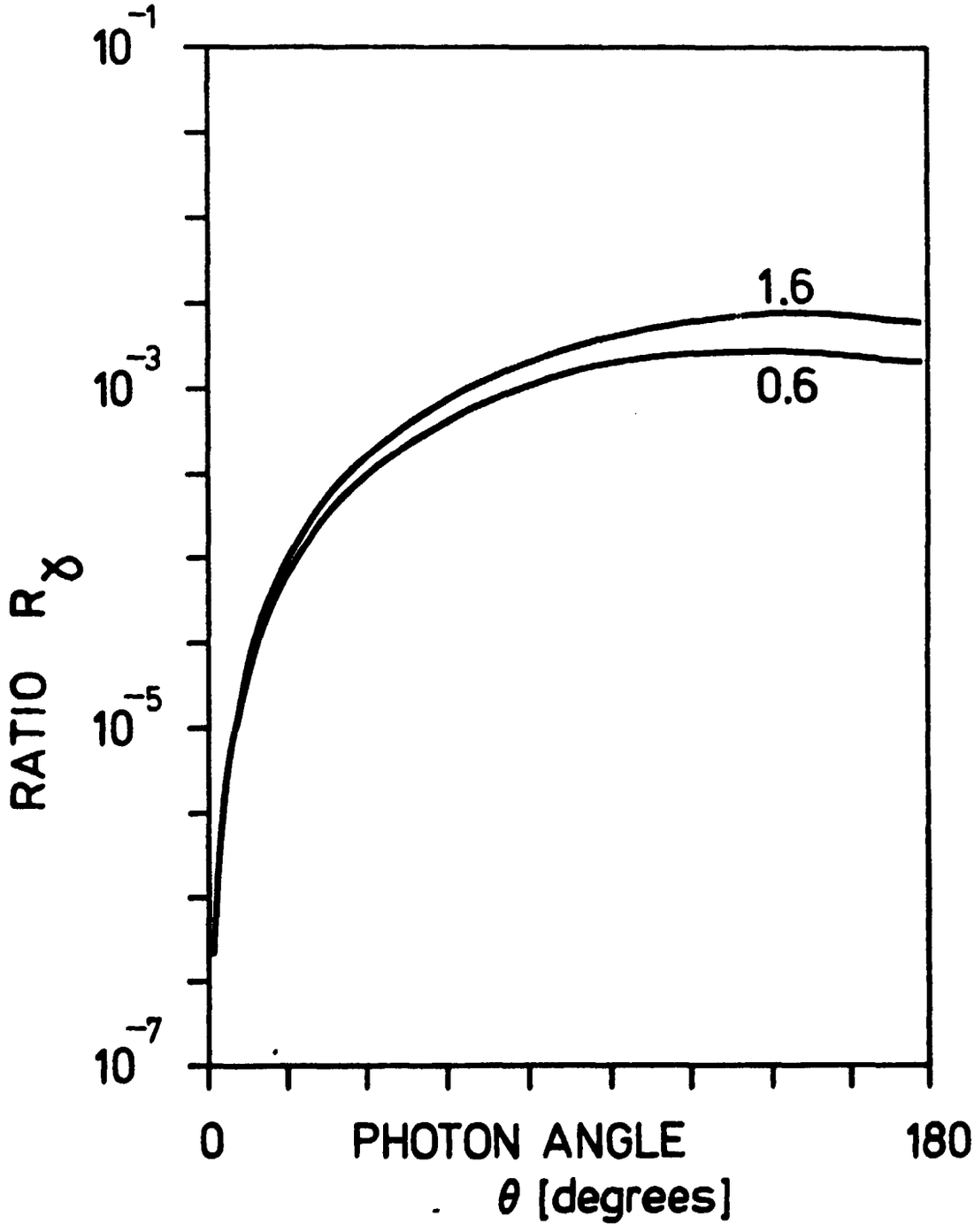
10^{-1}
10^{-3}
10^{-5}
10^{-7}
RATIO R_γ
1.6
0.6
0
PHOTON ANGLE
180
θ [degrees]

Fig. 6.

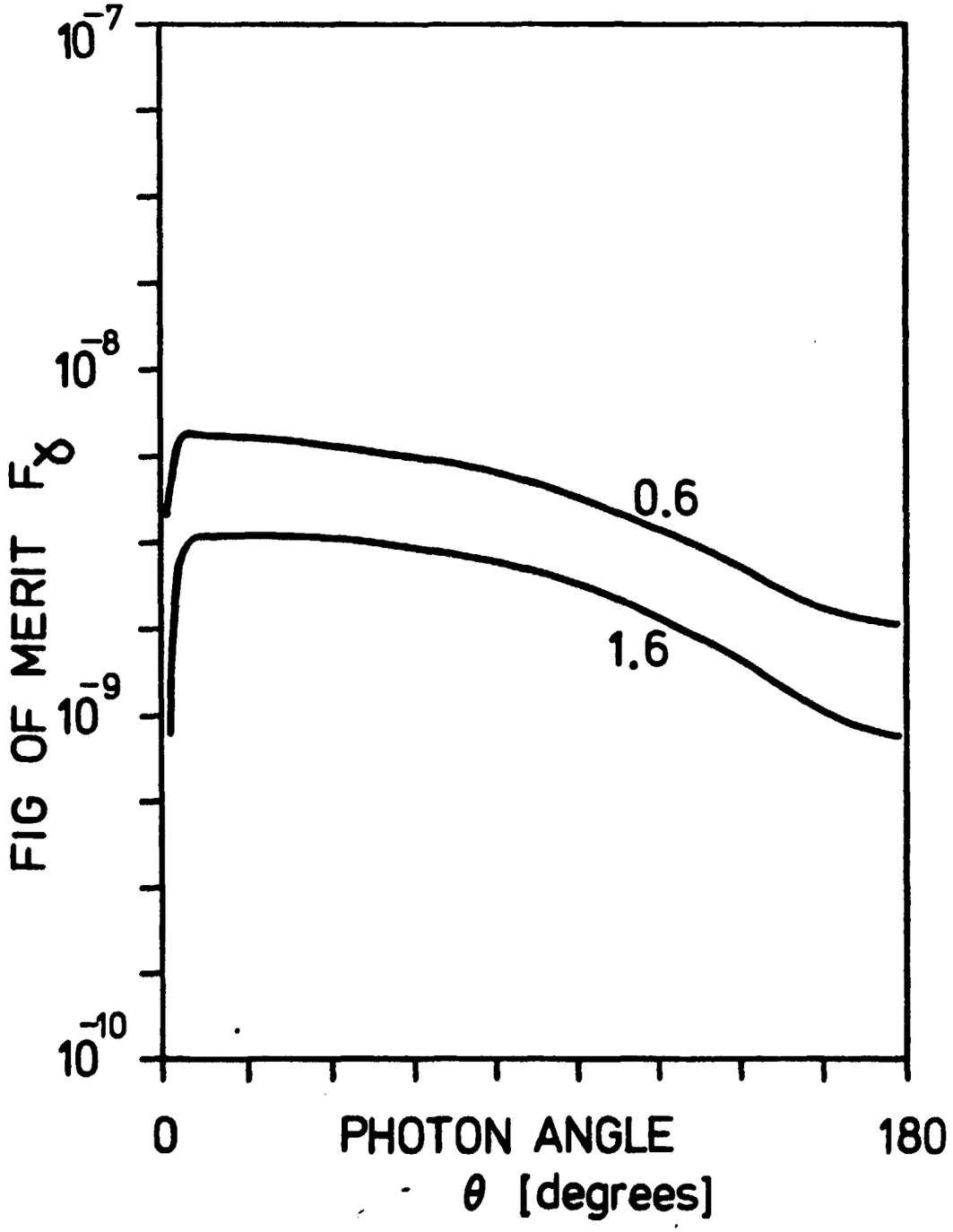
10^{-7}
10^{-8}
10^{-9}
10^{-10}
FIG OF MERIT F_γ
0.6
1.6
0
PHOTON ANGLE
180
θ [degrees]

Fig. 7.

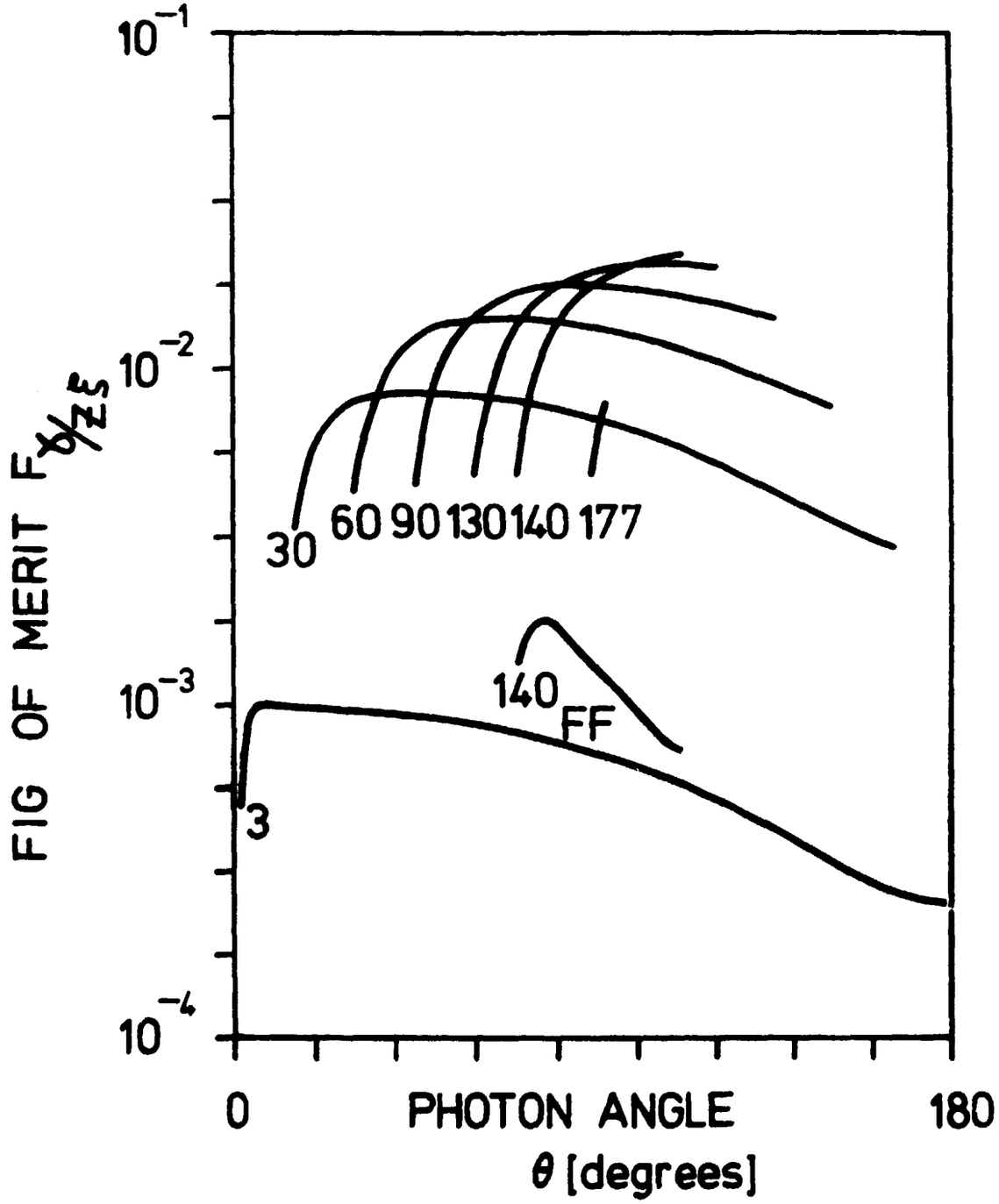
10^{-1}
10^{-2}
10^{-3}
10^{-4}
FIG OF MERIT $F_{\gamma/2\xi}$
30
60 90 130 140 177
140 FF
3
0
PHOTON ANGLE
180
θ [degrees]

Fig. 8.

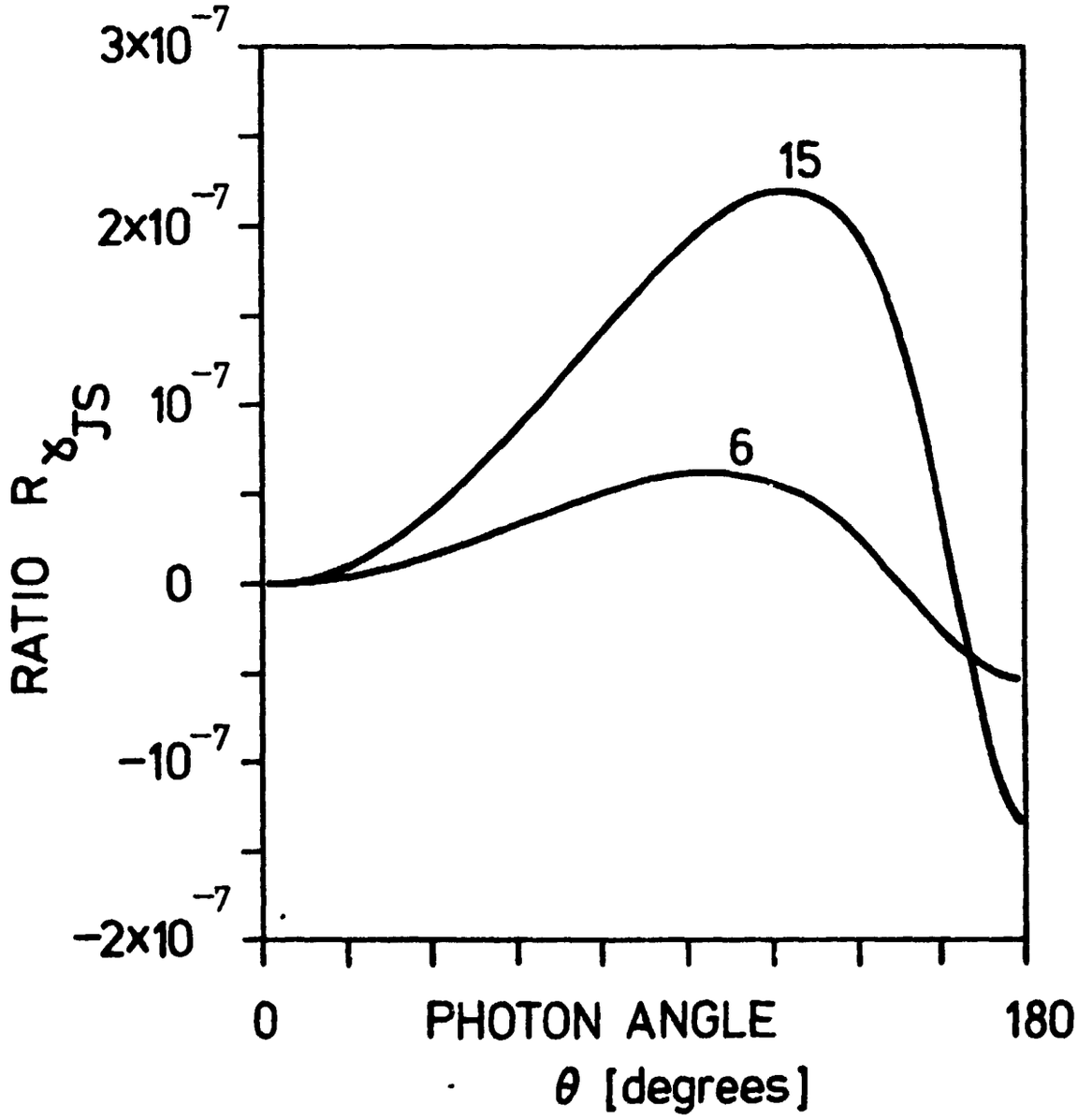
3x10^-7
2x10^-7
10^-7
0
-10^-7
-2x10^-7
RATIO R γJS
15
6
0
PHOTON ANGLE
180
θ [degrees]

Fig. 9.

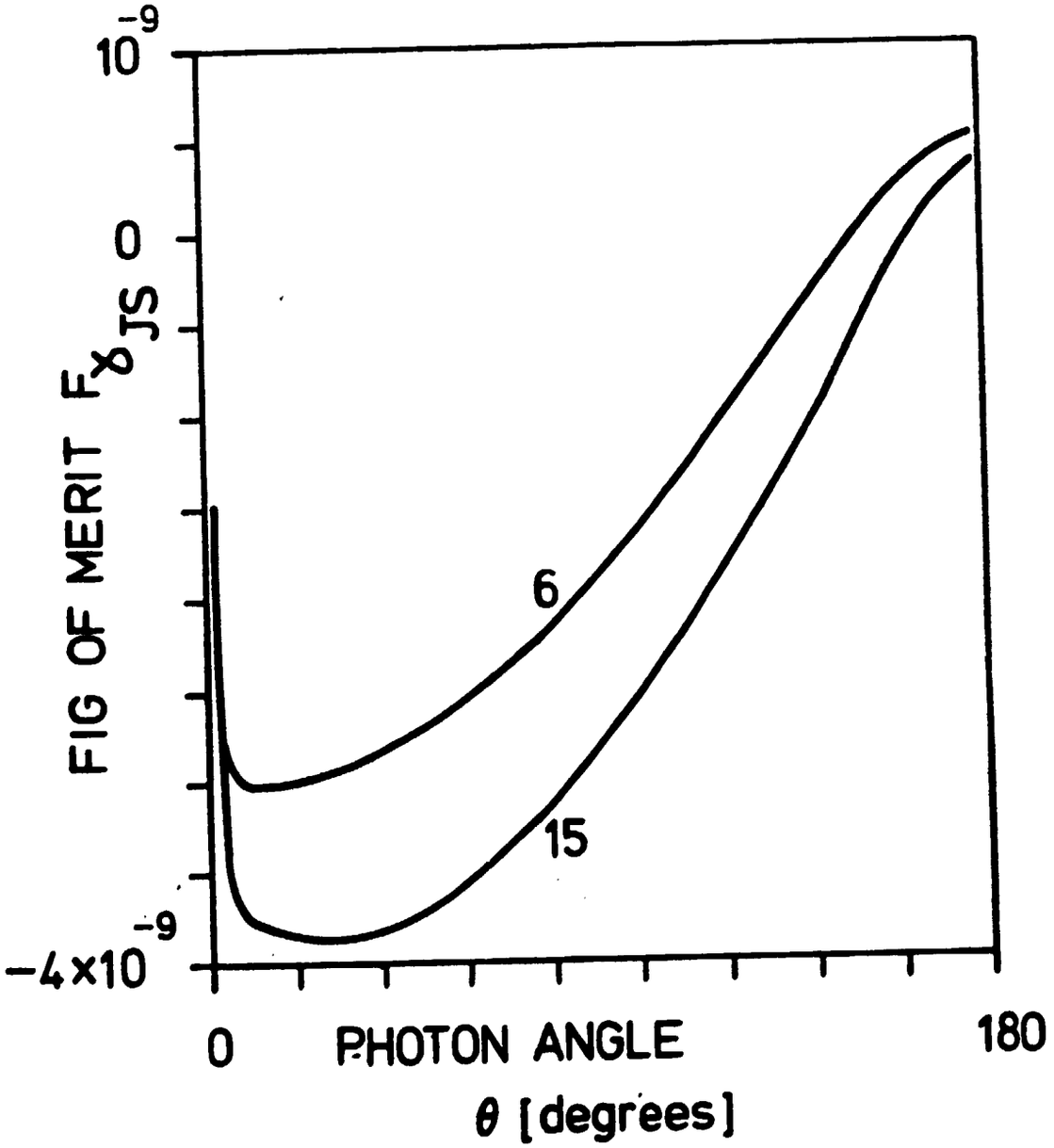
10^{-9}
0
-4×10^{-9}
FIG OF MERIT $F_{\gamma_{JS}}$
6
15
0
PHOTON ANGLE
180
θ [degrees]

Fig. 10.

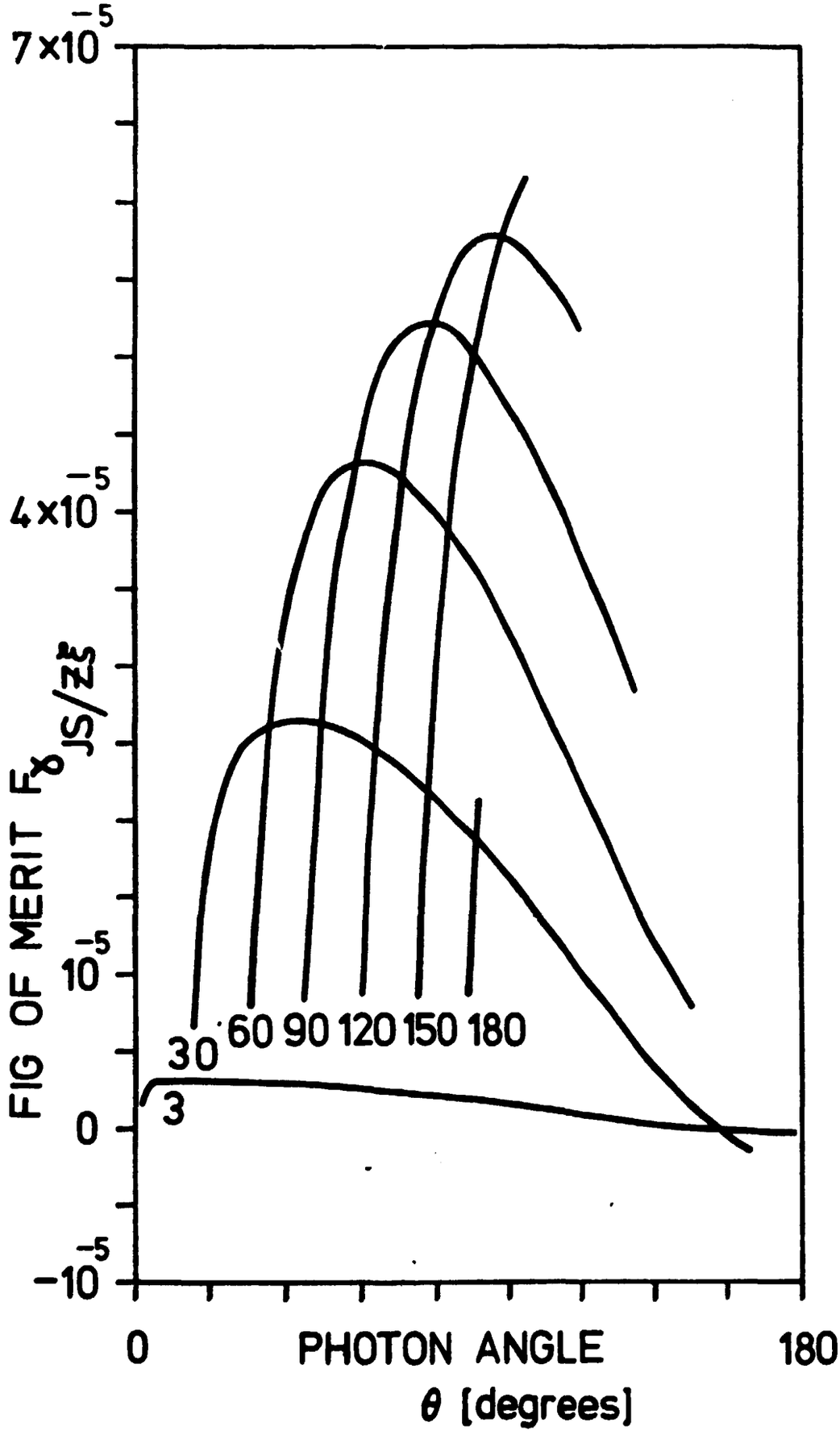
7×10⁻⁵
4×10⁻⁵
10⁻⁵
0
-10⁻⁵
FIG OF MERIT $F_{\gamma JS/Z\xi^2}$
30
60 90 120 150 180
3
0
PHOTON ANGLE
180
θ [degrees]

Fig. 11.